U.S. ARMY COMBAT CAPABILITIES DEVELOPMENT COMMAND – GROUND VEHICLE SYSTEMS CENTER

Characterization of Microstructure Associated with Adiabatic Shear in High-Mn, High-Al Steels

Dr. Katherine Sebeck

Specialist Research Engineer

Ground Vehicle Materials Engineering

WHAT IS FEMNAL?

- **High Mn, high Al low density steel with similar strength to RHA**
- **Weight and Performance**
  - 7.8 g/cc vs 2.7 g/cc vs 6.9 g/cc (steel vs Al vs FeMnAl)
  - Space considerations
  - Strength/Density vs Threat Performance/Density
    - **Going thinner is not necessarily better, or possible**
- **Army lightweighting is driven by meeting performance requirements for changing threats, new equipment, and maintaining logistic supports**
  - Army bridges, NATO rail car, and highway equipment transport trailer (HETT) designed for 70T capacity

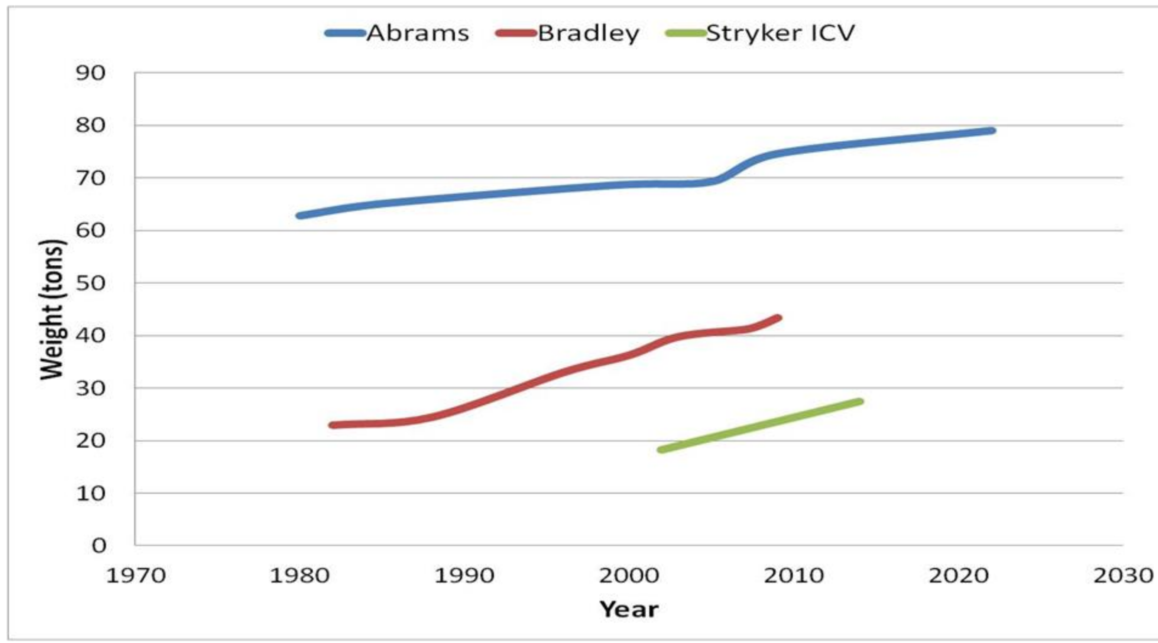

PROJECT MOTIVATION

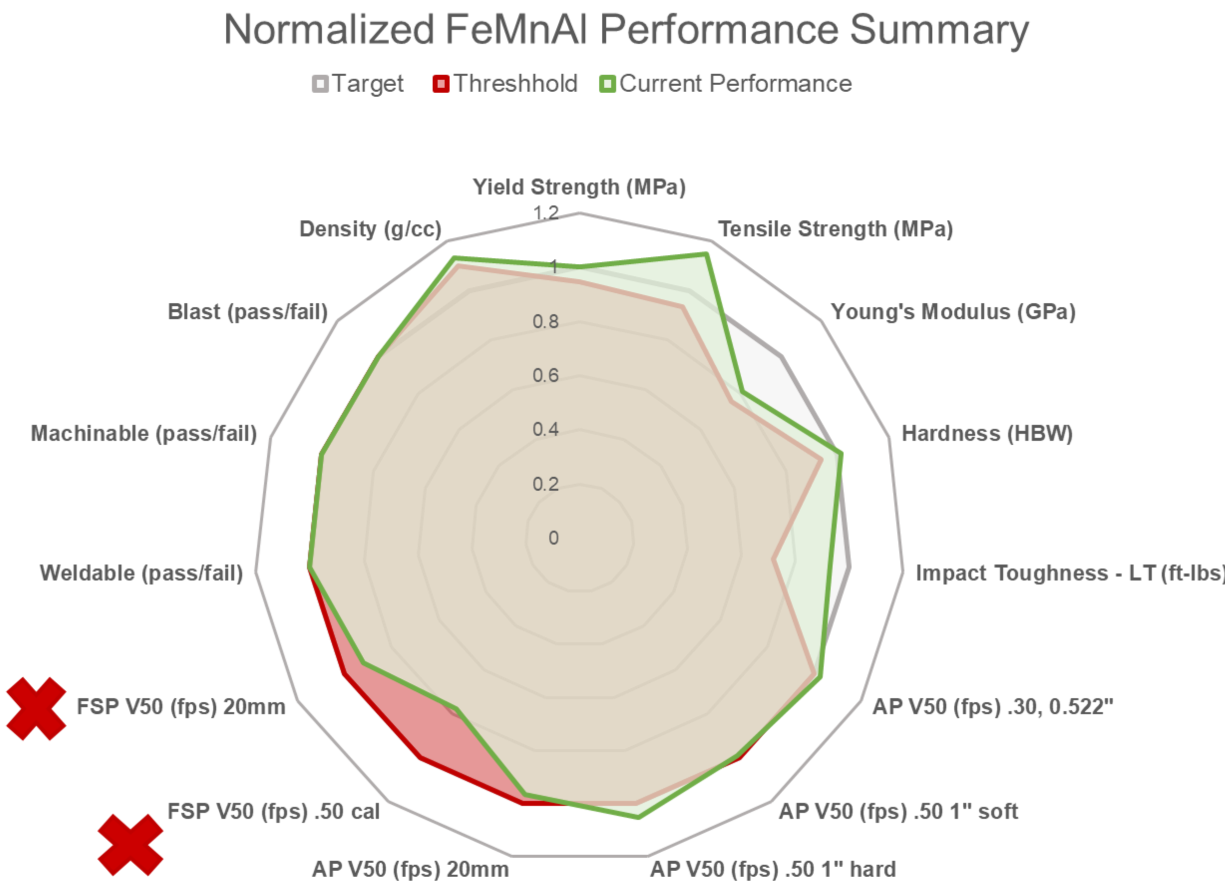

- **Generally met Class 1 RHA threats on a space efficiency basis, exceeded on a mass efficiency basis – influenced by hardness levels**
- **Underperformed against Class 2 RHA requirements on space efficiency basis; in line with Class 1 for mass efficiency – no apparent effect of hardness or impact toughness**

ADIABATIC SHEAR

- **Adiabatic Shear**
  - The onset of shear banding occurs when thermal softening overcomes strain and strain-hardening effects
    - Higher hardenability and lower thermal softening lead to improved resistance to shear localization

$$\frac{d\tau}{d\gamma} = \left(\frac{\partial\tau}{\partial\gamma}\right)_{\dot{\gamma},T} + \left(\frac{\partial\tau}{\partial\dot{\gamma}}\right)_{\gamma,T}\frac{d\dot{\gamma}}{d\gamma} + \left(\frac{\partial\tau}{\partial T}\right)_{\gamma,\dot{\gamma}}\frac{dT}{d\gamma} \leq 0$$

  - Neglecting strain-rate hardening, the critical shear strain for shear localization can be expressed as:

$$\gamma_c = \frac{\rho C_p n}{-\frac{\partial\tau}{\partial T}}$$

    - Where ρ is density, C_P is specific heat capacity, *n* is strain-hardening index, and –δτ/δT is the thermal-softening parameter

Adiabatic heating in high strain rate events occurs because energy is unable to leave the system in the time frame of the work done by the event

- **Looking for evidence of dynamic recrystallization**
  - Some may be in the base microstructure due to wrought processing, incomplete solution treatment
- **Shear bands should follow flow lines of material displaced by projectile**

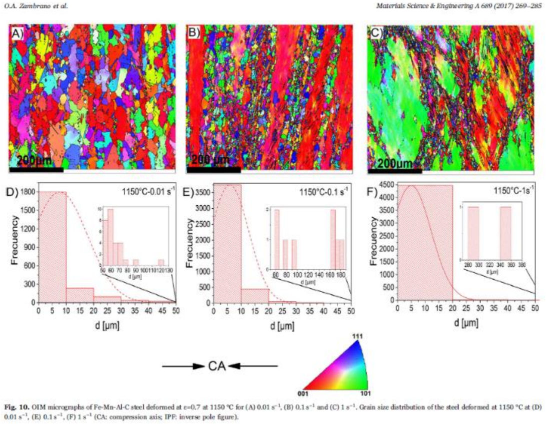

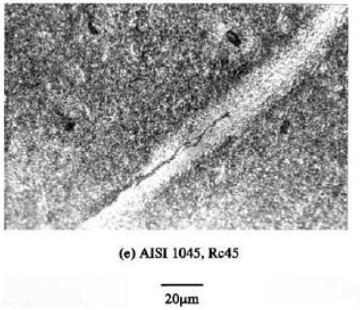

O.A. Zambrano *et. al.*, "Hot deformation of a Fe-Mn-Al-C steel susceptible of κ-carbide precipitation" Mat Sci Eng A 689 pp 269-285 (2017)

Hu, CJ and Lee, PY. "Ballistic Performance and Microstructure of Modified Rolled Homogeneous Armor Steel". J. Ch. Inst. Eng 25 (1) pp 99-107 (2002)

BALLISTIC THEORY

- **Steel is typically well described by the Culver equation for failure strain:**

$$\epsilon_i = \frac{\rho c n}{-\left.\frac{\partial \sigma}{\partial T}\right|_{\epsilon,\dot{\epsilon}}}$$

ϵ_i = failure strain

ρ = density

c = specific heat capacity

n = strain hardening exponent

$\left.\frac{\partial \sigma}{\partial T}\right|_{\epsilon,\dot{\epsilon}}$ = change in stress as a function of temperature for constant strain and strain rate

However, this equation significantly overpredicts FeMnAl performance

- **Aluminum is more well described by the Grady criterion for adiabatic shear localization**

$$\Gamma_{c0} = \frac{\rho c}{\alpha}\left(\frac{9\rho^3 c^2 \chi^3}{\sigma_y^3 \alpha^2 \dot{\epsilon}}\right)^{1/4}$$

Γ_{c0} = fracture energy

ρ = density

c = specific heat capacity

α = linear thermal softening

χ = thermal conductivity

σ_y = yield strength

$\dot{\epsilon}$ = strain rate

  – Based on projected thermal properties, this model more accurately predicts FeMnAl performance

	RHA	Estimated FeMnAl Properties	Measured FeMnAl Properties
Culver	1	3.4x	7.8x
Grady	1	0.49x	1.2x
Fragment Simulating Projectile	--	--	0.65x

- **Four key parameters are related to shear localization:**
  - Specific heat capacity
  - Thermal Conductivity
  - Linear Thermal Softening
  - Density

$$\Gamma_{c0} = \frac{\rho c}{\alpha}\left(\frac{9\rho^3 c^2 \chi^3}{\sigma_y^3 \alpha^2 \dot{\epsilon}}\right)^{1/4}$$

Γ_{c0} = fracture energy
ρ = density
c = specific heat capacity
α = linear thermal softening
χ = thermal conductivity
σ_y = yield strength
$\dot{\epsilon}$ = strain rate

These are all affected by the aluminum content in FeMnAl

- **Additional aluminum leads to a dilation in the lattice parameter of the main austenitic phase**
  - Changes lattice vibrations, number of conduction electrons
  - Atomic radius of Al is 1.43Å, Fe is 1.24Å
  - Atomic mass of Al 26.98u, Fe is 55.84u

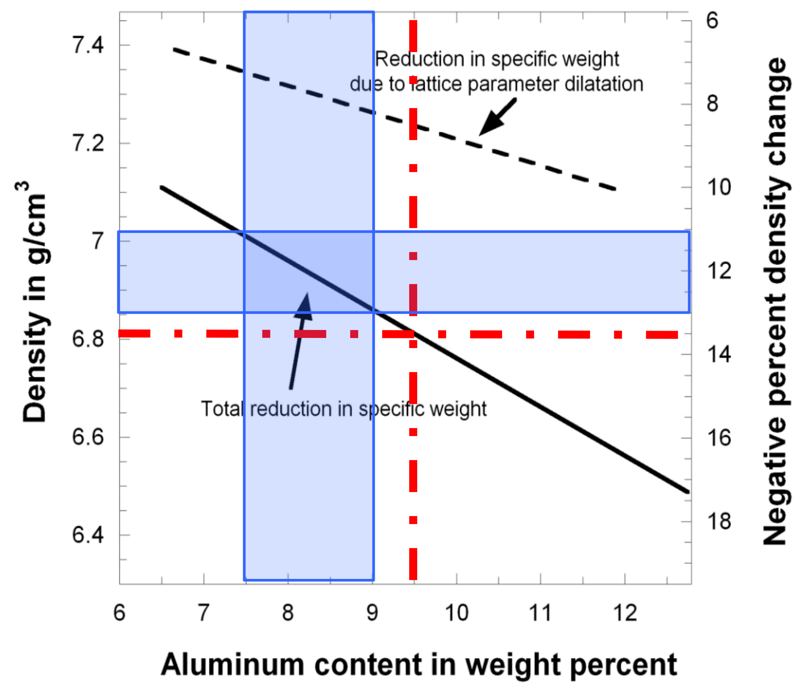

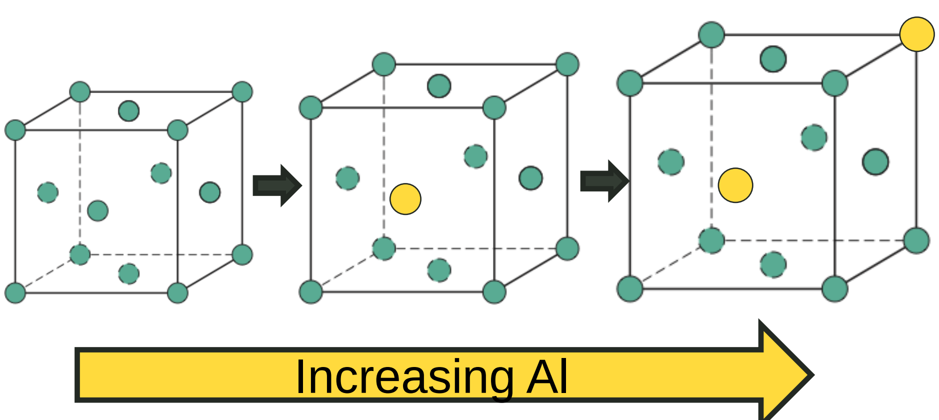

COMPOSITIONAL STUDY EFFORT

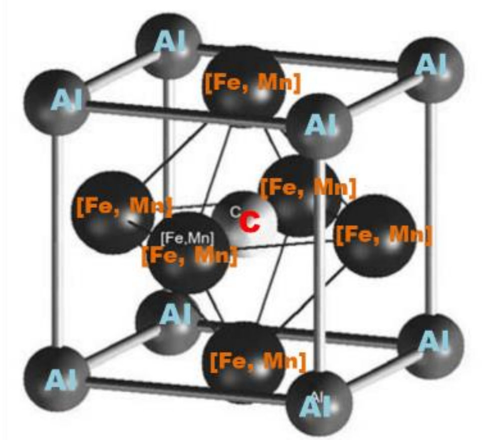

κ-carbide cubic perovskite crystal structure (E2₁)

Level	Mn (wt%)	Al (wt%)	C (wt%)
Low	25.0	8.0	0.8
High	29.0	9.0	0.9

	Mn (wt%)	Al (wt%)	C (wt%)	Mo (wt %)	V (wt %)
No Mo	29.0	9.0	0.90	0.0	0
Hi Mo	29.0	9.0	0.90	0.75	0
Low Al 1	25.0	7	0.90	0.55	0
Low Al 2	25.0	7	0.80	0.55	0
V	29.0	9	0.90	0.55	0.55

- Building on previous design of experiments to evaluate sensitivity of toughness and aging to composition
  - 2 level full factorial for Mn, Al and C
    - Main components of the carbide which controls hardness, toughness
  - 5 separate compositions to evaluate the role of grain refiners, lower Al levels
- Two different producers, small plates
  - Missouri S&T using traditional sand casting
  - Arcelor Mittal using Vacuum Induction Melting (VIM)

BALLISTIC AND CVN PERFORMANCE RESULTS

- **No clear correlation between impact test performance and fragment simulating projectile defeat**
- **Overall trend in V50 follows plates thickness**
  - Widest variation in performance at 0.53" thick plate
- **FSP normalized to Sample 20**

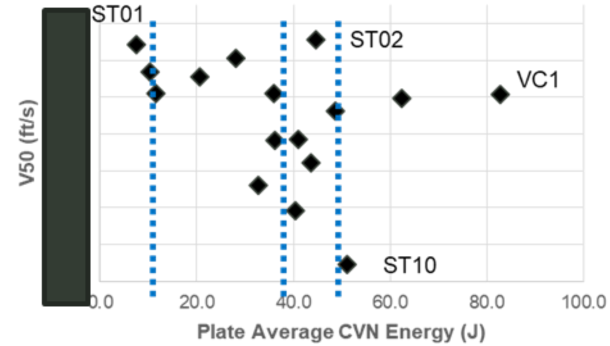

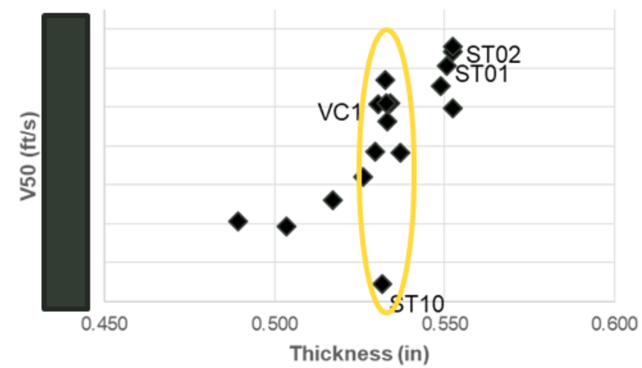

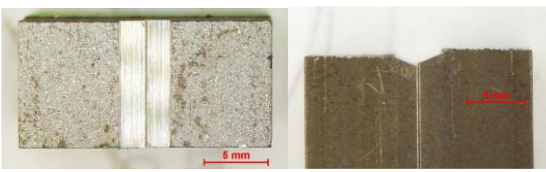
ST01: t=0.553, CVN=7.6J , V50=1.02x

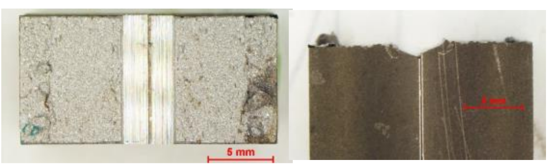
ST02: t=0.553, CVN=44.7J, V50=1.03x

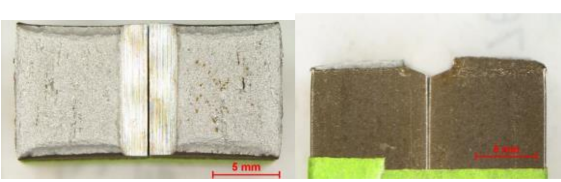
ST10: t=0.532, CVN=51.0, V50= 0.83x

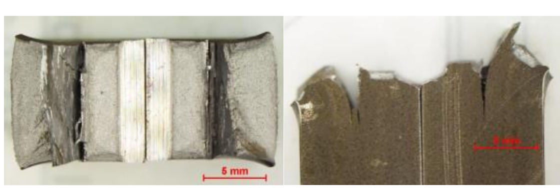
VC1: t=0.53, CVN= 82.7, V50= 0.98x

Identified 5 samples based on CVN, ballistic performance for detailed analysis

Sample ID	02 (VC1)	06 (VC9)	08 (VC11)	20 (ST9)	21 (ST10)
Nominal Composition	27.3Mn-8.75Al-0.95C-0.9Si-0Mo	23.1Mn-8.94Al-0.88C-0.93Si-0.42Mo	26.9Mn-8.85Al-0.84C-0.97Si-0.48Mo	24.9Mn-7.5Al-1.1C-0.88Si-0.48Mo	24.55Mn-6.59Al-1.06C-0.79Si-0.48Mo
CVN Energy (J)	41.0	48.6	36.2	10.3	51.0
Normalized FSP V50	0.94	0.96	0.94	1	0.83
Plate Thickness (in)	0.53	0.533	0.537	0.533	0.532

WORK UNDER THIS ILIR

- **Fracture inspection**
- **Optical Microscopy**
  - Base material
  - Partial penetration
  - Complete penetration
- **Density**
- **Thermal Conductivity**
- **Electron Backscatter Diffraction**

Complete Penetration (CP)

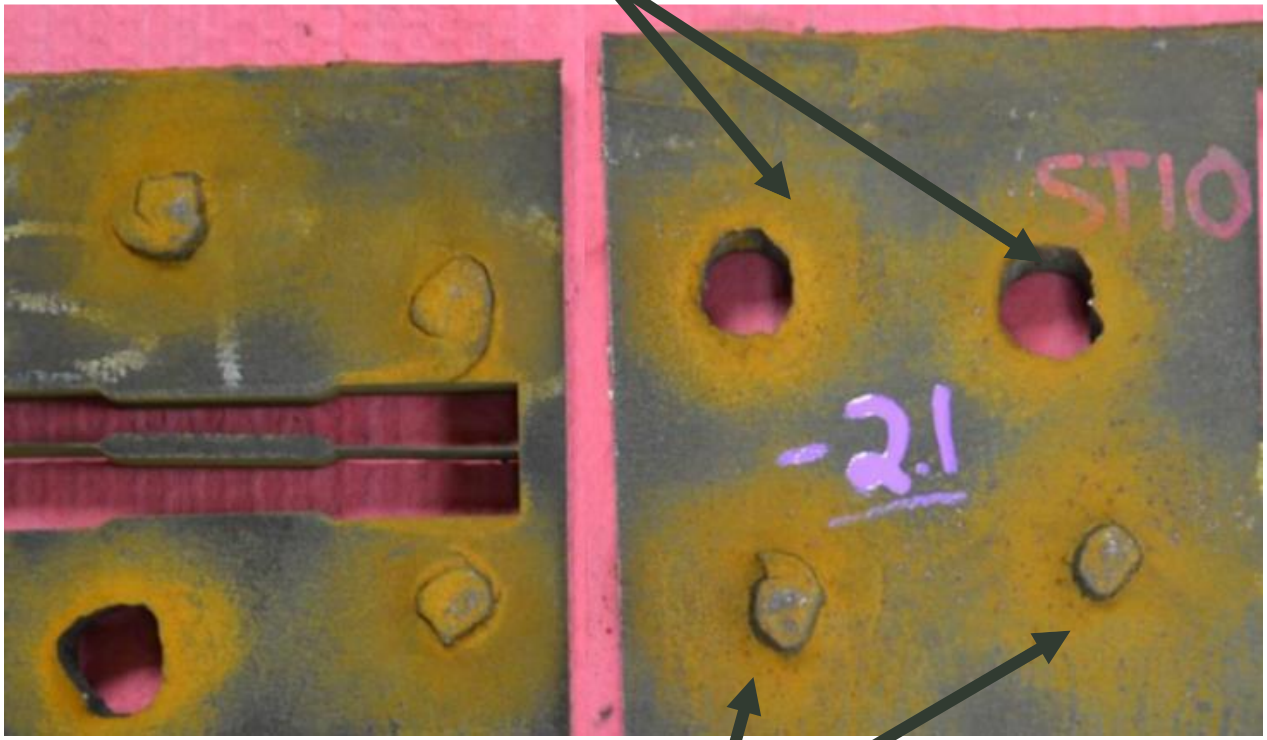

Partial Penetration (PP)

TENSILE PROPERTIES

- **Hardness below target of 320 HBN**
- **Lower Mn level was not detrimental to yield strength**
  - Strength dominated by heat treatment kinetics, achievable at a wide range of compositions

Sample ID	Yield Strength (MPa)	Tensile Strength (MPa)	Elongation (%)	Surface Hardness (HBN)	Core Hardness (HBN)	Measured Composition		
						Mn	Al	C*
VC3-02	969	1116	45.7	253	257	25.4	7.46	0.93
VC9-06	1040	1224	43.7	263	262	22.1	7.5	0.92
VC11-08	1309	1490	41.8	264	259	25.8	7.42	0.83
ST9-20	Not enough material to complete tensile testing			237	271	25.4	7.1	1.21
ST10-21				214	259	28.2	8.6	0.83

INCLUSIONS AND FRACTURE SURFACES

- **Majority of inclusions are:**
  - AlON
  - MnS
- **Based on location on fracture surfaces, not substantially impacting the fracture performance**

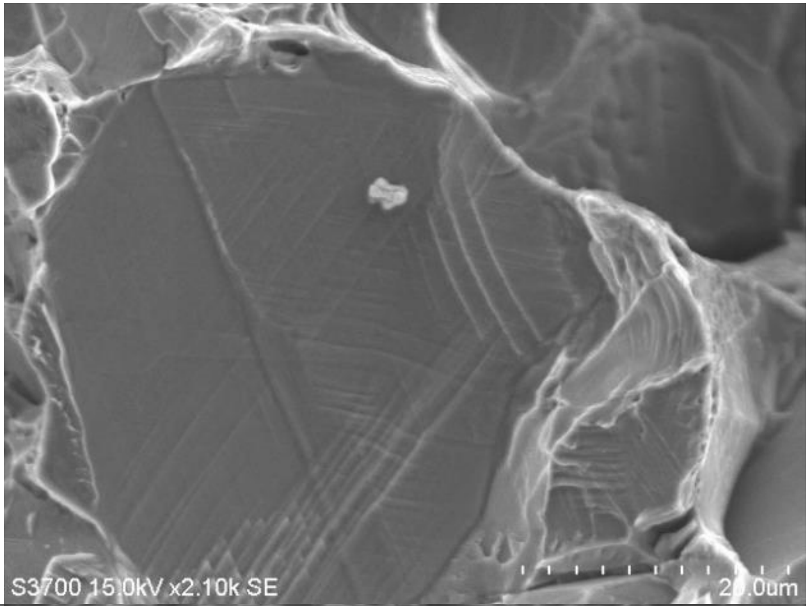

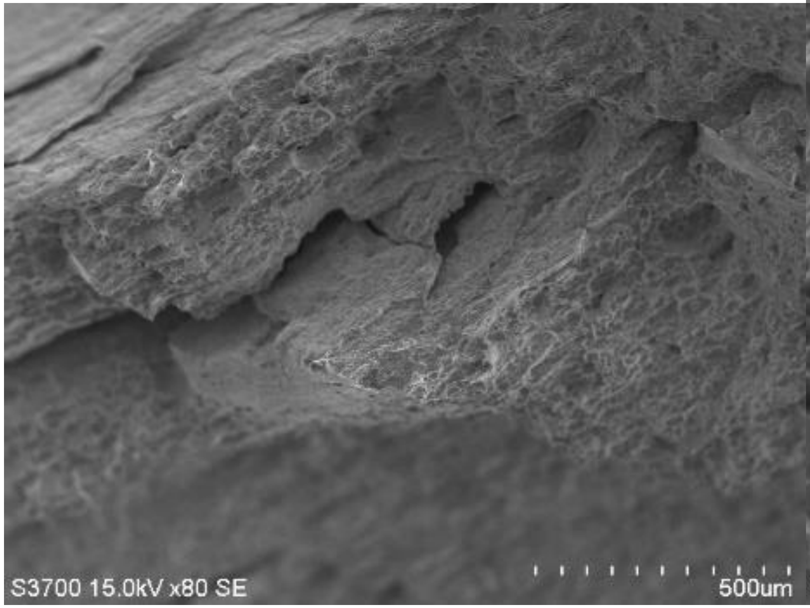

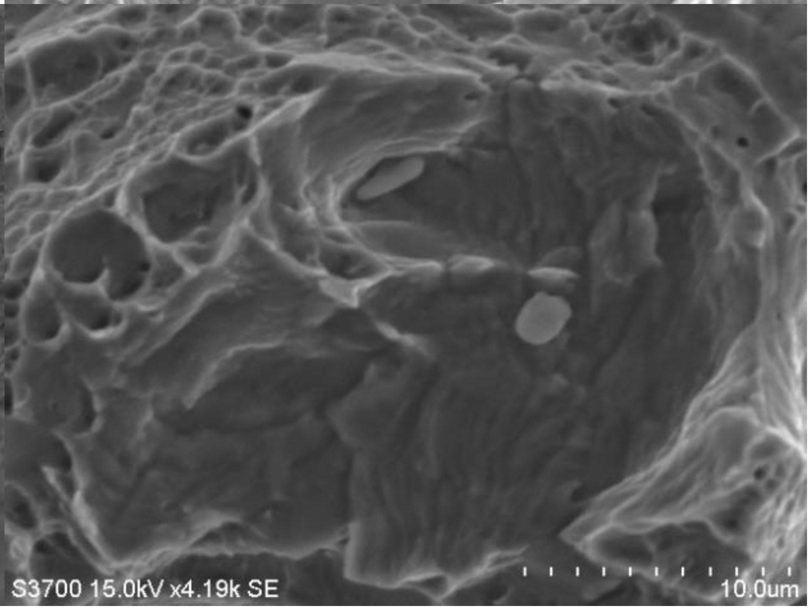

OPTICAL MICROSCOPY

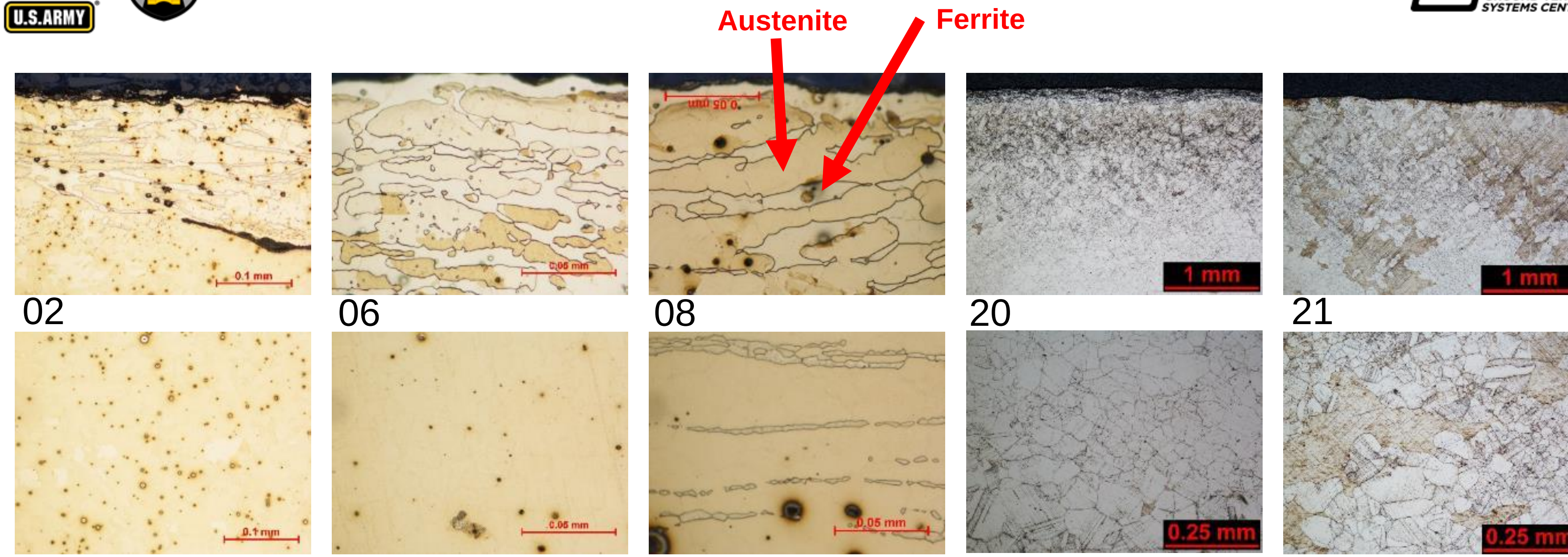

5% Nital etch

- **Some ferrite is observed at the plate surface for all compositions**
  - This is attributed to decarburization during rolling and subsequent heat treatment
  - 08 also shows some ferrite stringers in the center line (below)
  - Centerline believed to be due to incomplete solution treatment
- **More uniform grain size observed in plates produced by vacuum induction melting**
  - Significant annealing twinning observed
- **Significant microporosity throughout the structure**

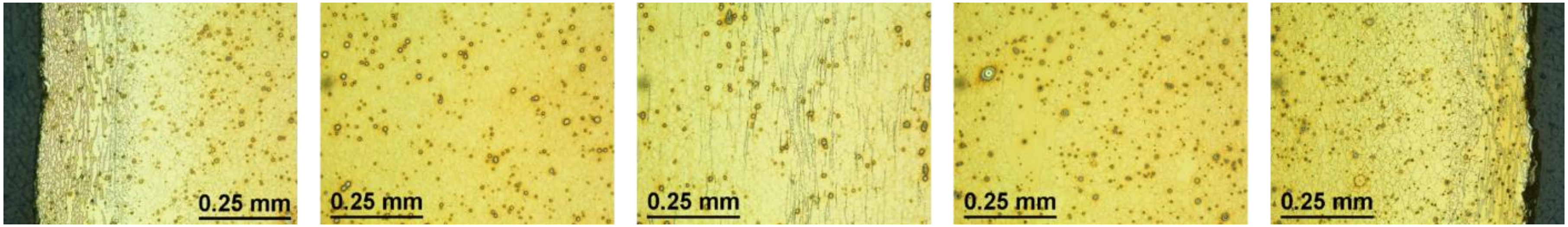

08

BASE MICROSTRUCTURE

- **Larger, equiaxed grains in the sand castings (20 and 21) vs VIM castings (2,6 and 8)**
- **Less residual ferrite in the sand cast samples**

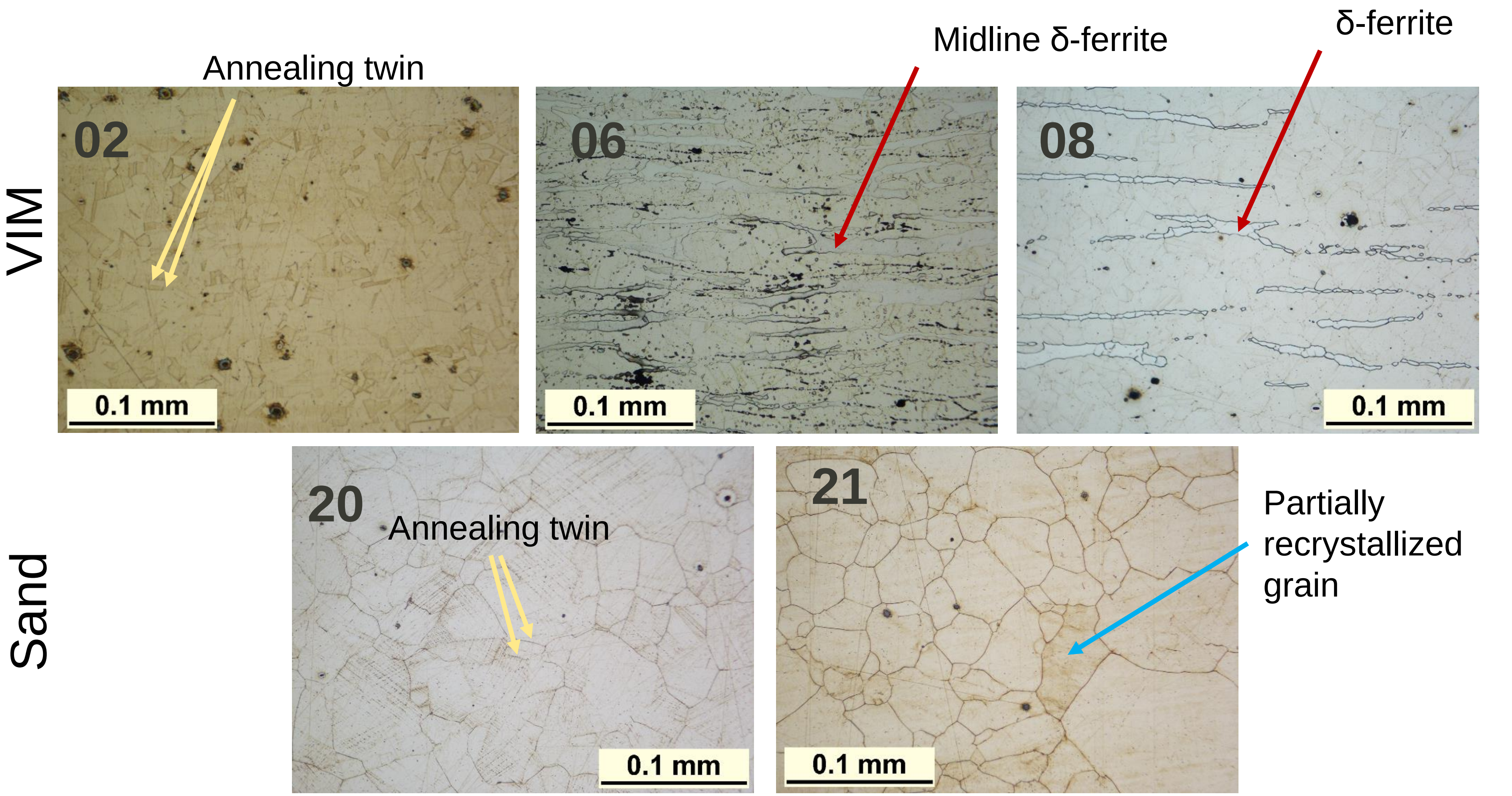

IMPACT FRACTURE PROFILE

VIM

Sand

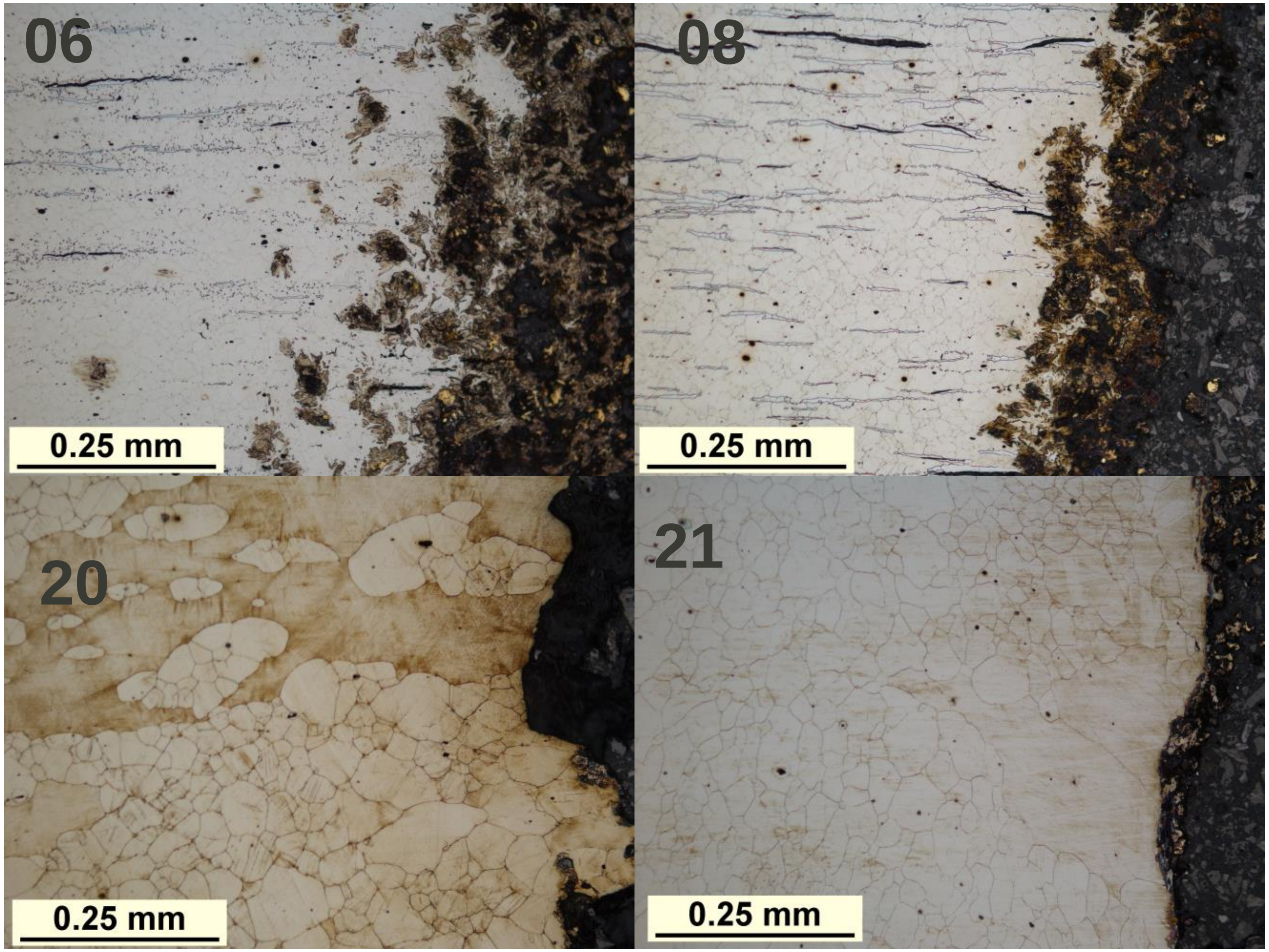

- **Cross section of samples from Charpy V Notch impact testing**
- **VIM cast samples have more ragged fracture surface**
  - Intergranular fracture in austenitic regions
  - Intragranular fracture through ferrite grains
    - Confirms anticipated detrimental influence of ferrite
  - Intragranular fracture through large incompletely recrystallized grains (see 20)

LOW MAGNIFICATION PARTIAL PENETRATION FRACTURES

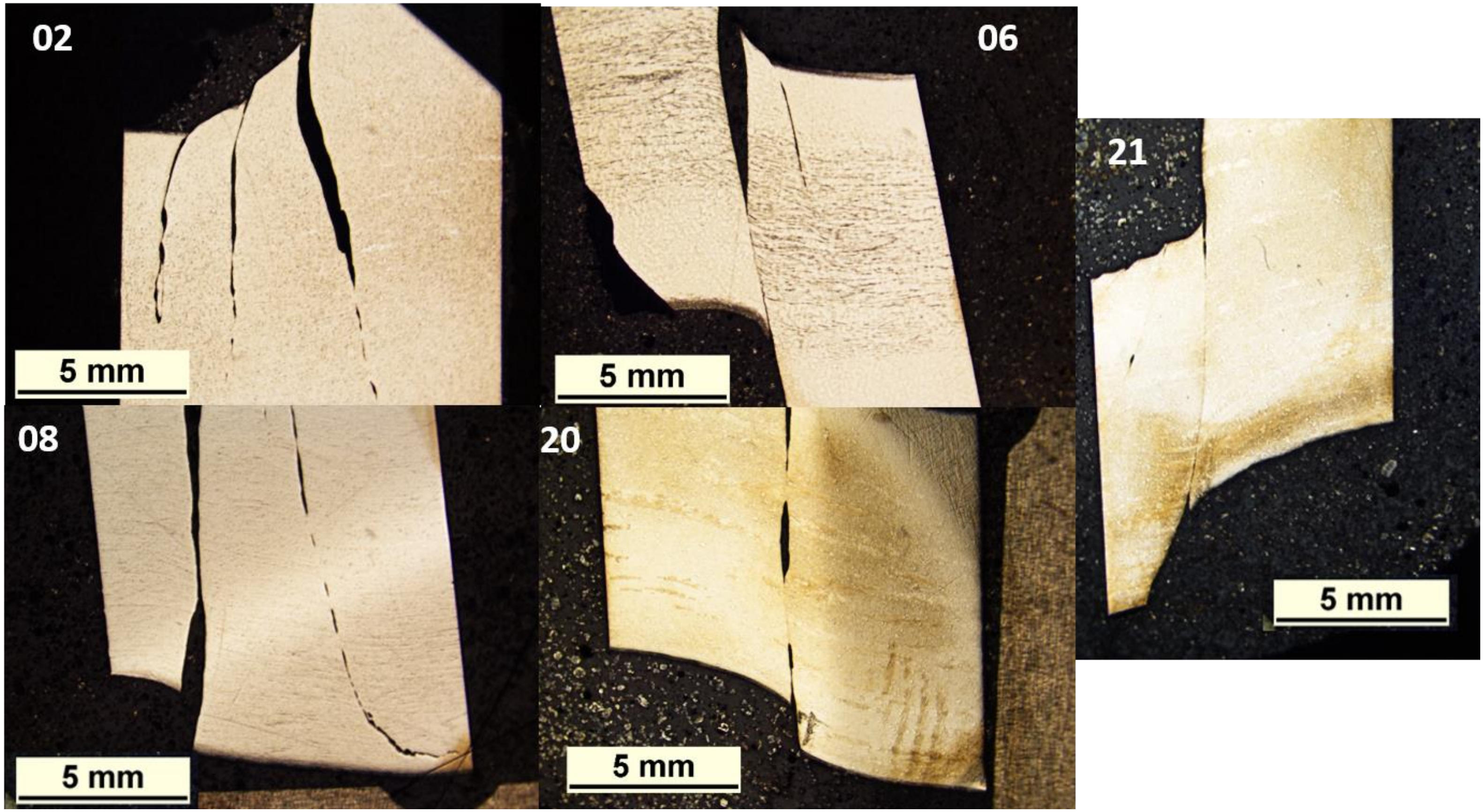

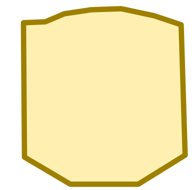

Projectile profile

- **Compound fracture paths driven by projectile profile**
  - Additional stress concentrations leading to additional fracture paths
  - This may be driving the spiral pattern in the fracture

PARTIAL PENETRATION

VIM

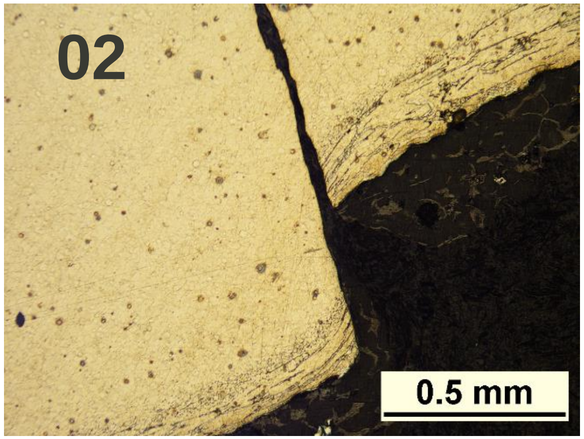

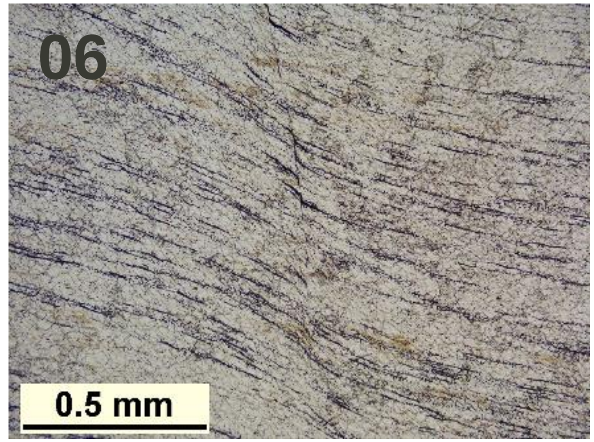

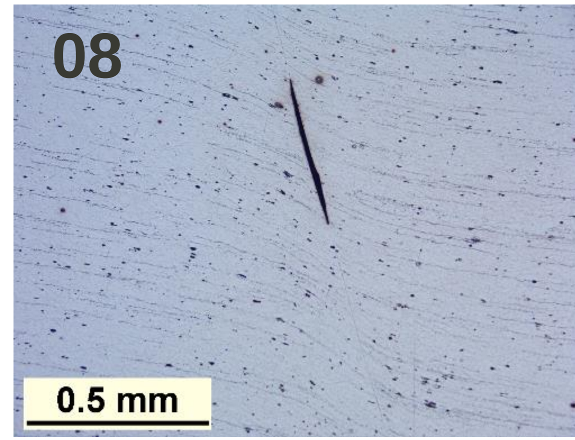

Sand

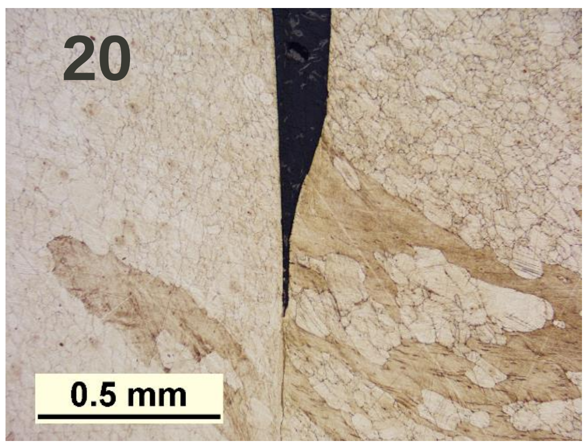

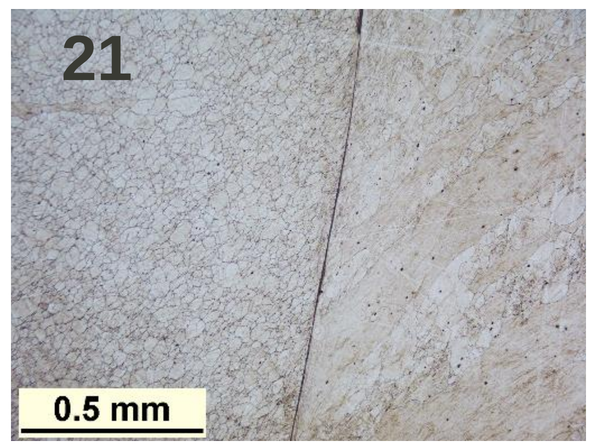

- **Flow of microstructure visible on either side of the fracture path**
  - Smaller grains seem to be flowing
  - Large unrecrystallized grains failing intragranularly, ferrite failing intragranularly
- **Less flow before shear than anticipated from other steels**
- **No transformation band as seen in martensitic steels as the structure is already austenitic**

06

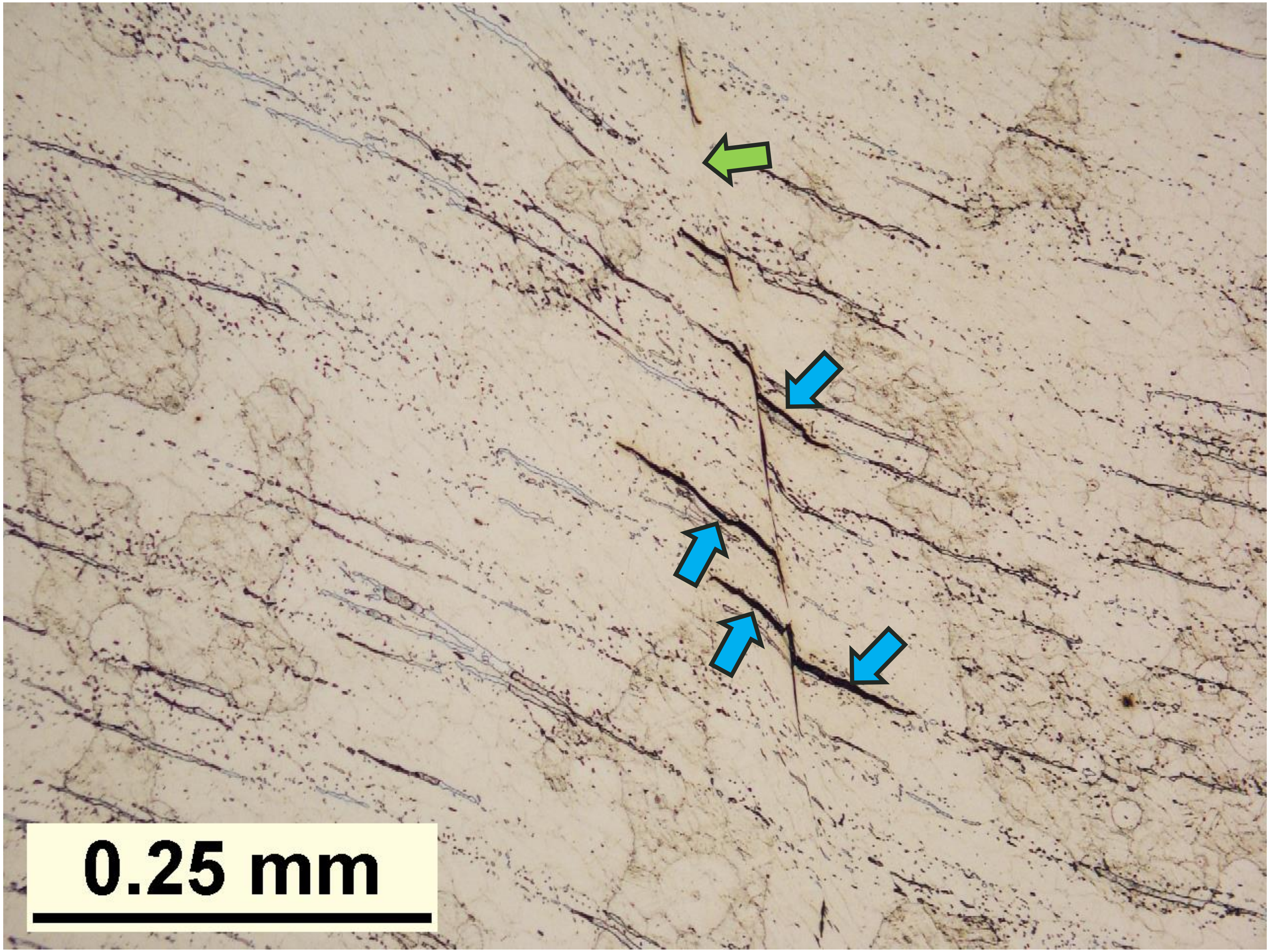

CLEAVAGE OF GRAINS

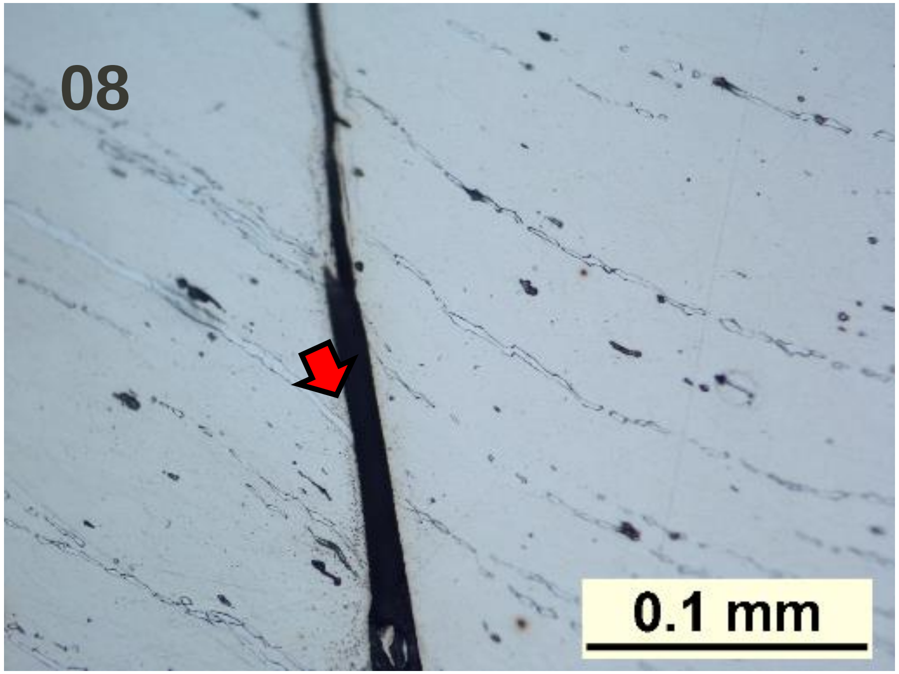

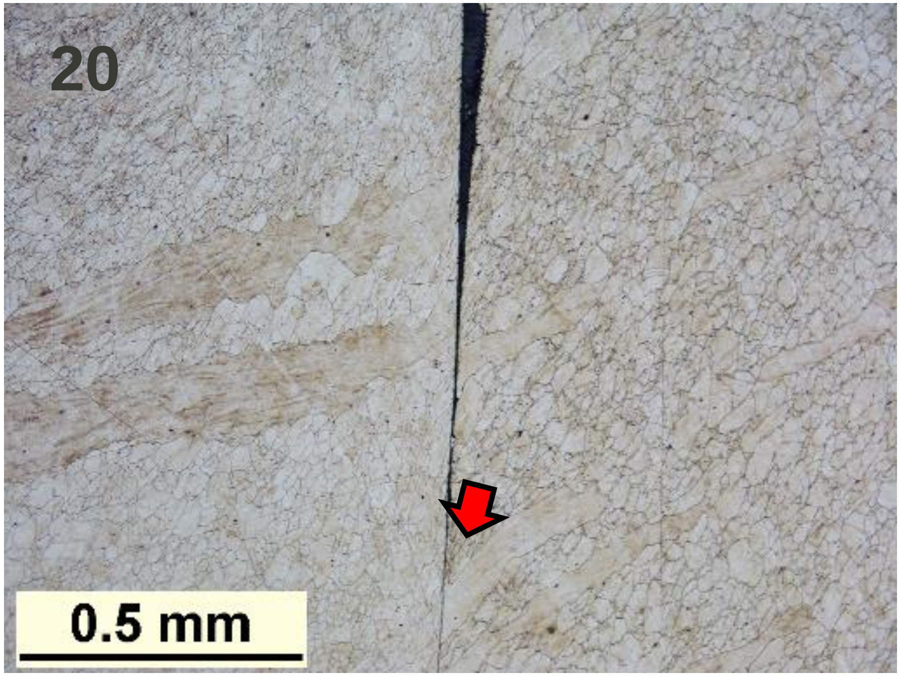

COMPLETE PENETRATION

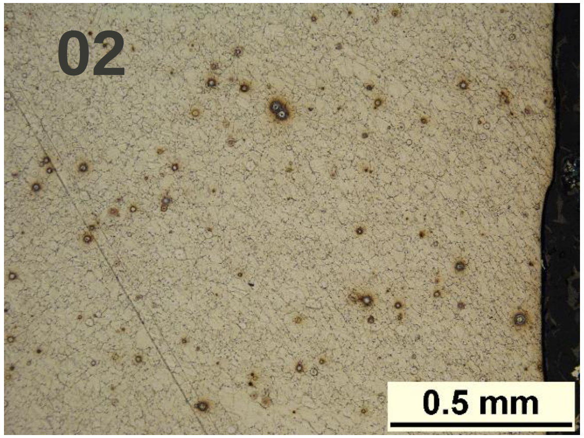

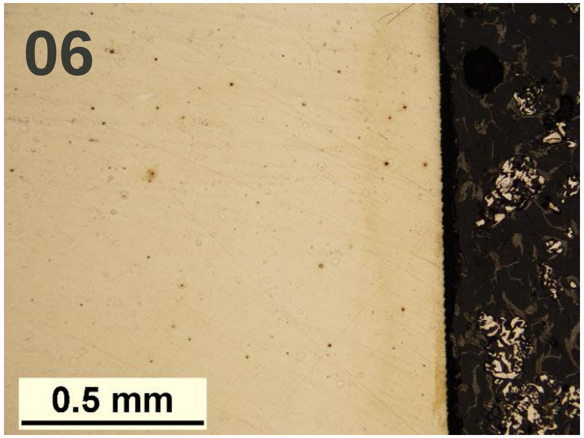

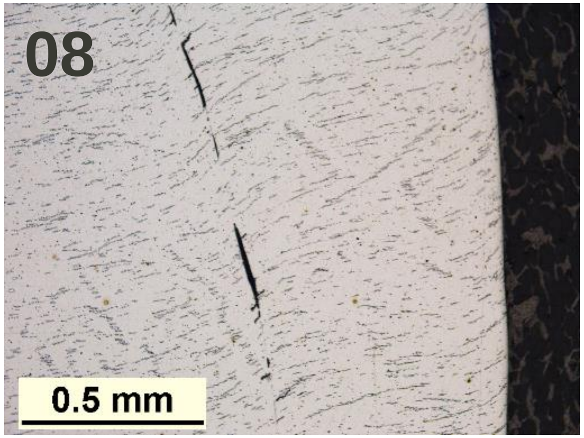

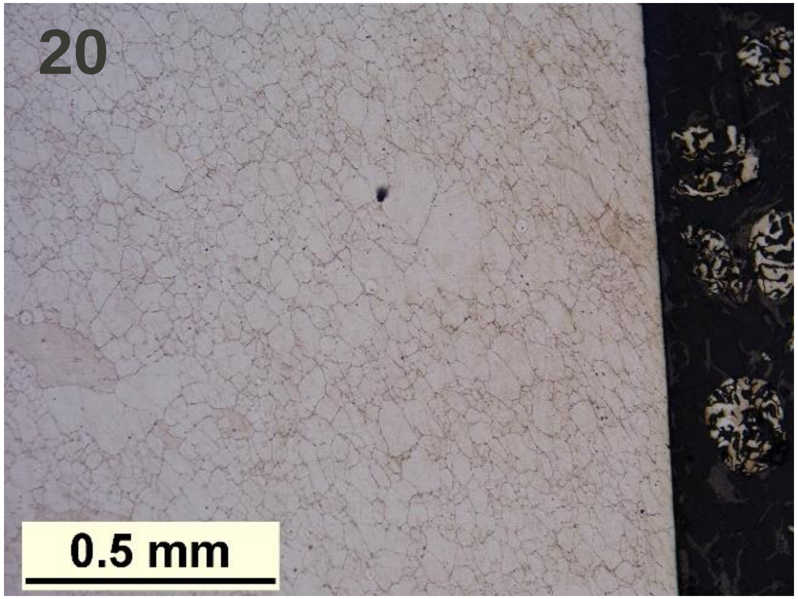

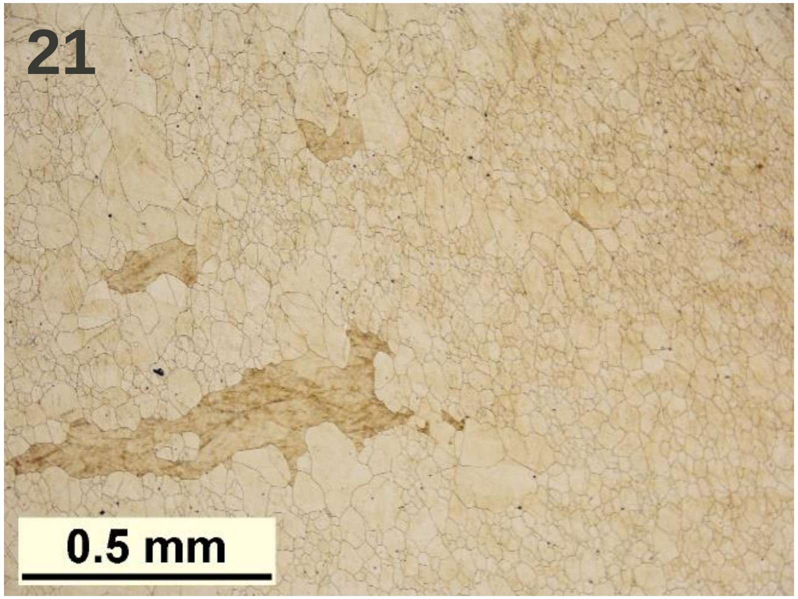

- **Grain refinement and deformation at penetration surface**

COMPARISON BETWEEN CONDITIONS

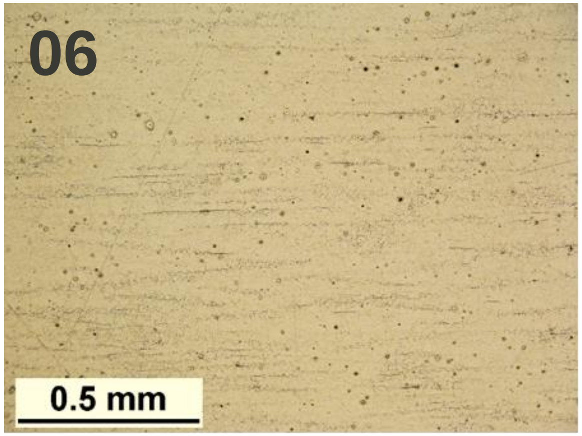

Base

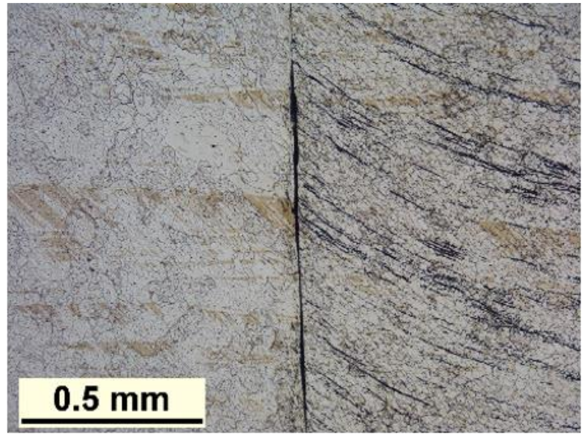

Partial Penetration

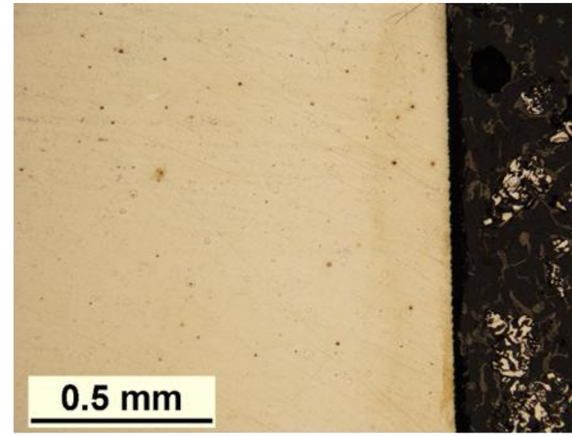

Complete Penetration

- Equiaxed austenite
- Laminar ferrite stringers
- Porosity but no cracks

- Skewed austenite
- Curved ferrite stringers
- Cracking along ferrite grains

- Skewed austenite, refined grains
- Curved ferrite stringers
- Cracking along ferrite grains

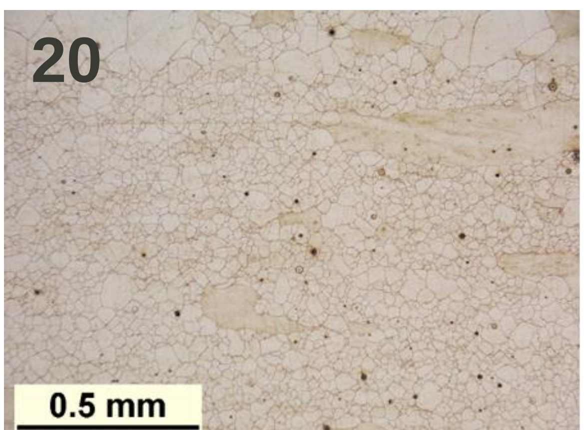

Base

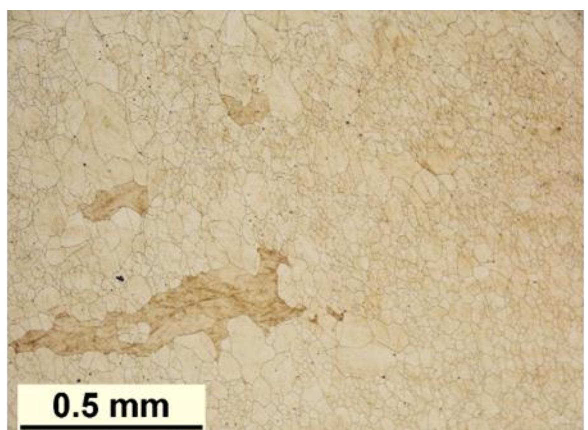

Partial Penetration

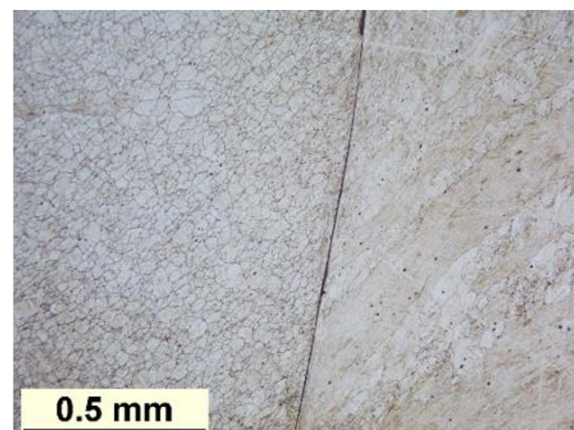

Complete Penetration

EBSD CHALLENGES

- **Sample preparation issues**
  - Selective etching of grain boundaries by polishing media, partially resolved via alternative cleaning methods
- **Charge build up leading to lateral drift (green arrow)**
  - Trying ion milling and gold sputter coating once gas canisters installed in new lab space
- **Lack of coherent pattern due to unrecrystallized grains, damage (yellow arrows)**
- **Older equipment**
  - Scans take 10s of hours to complete vs 10s of minutes on newer equipment

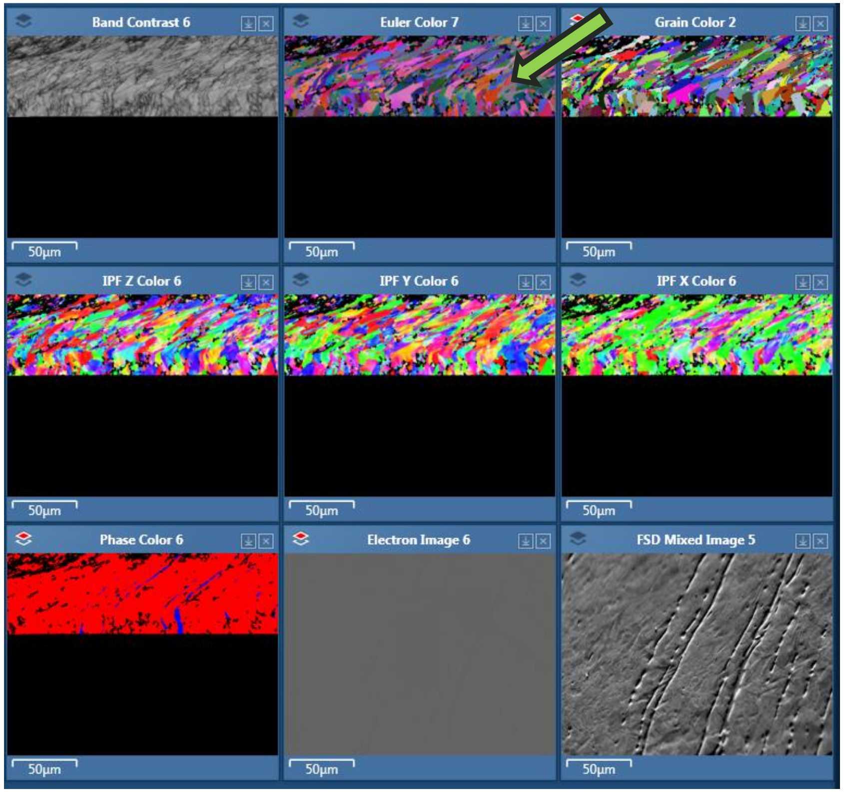

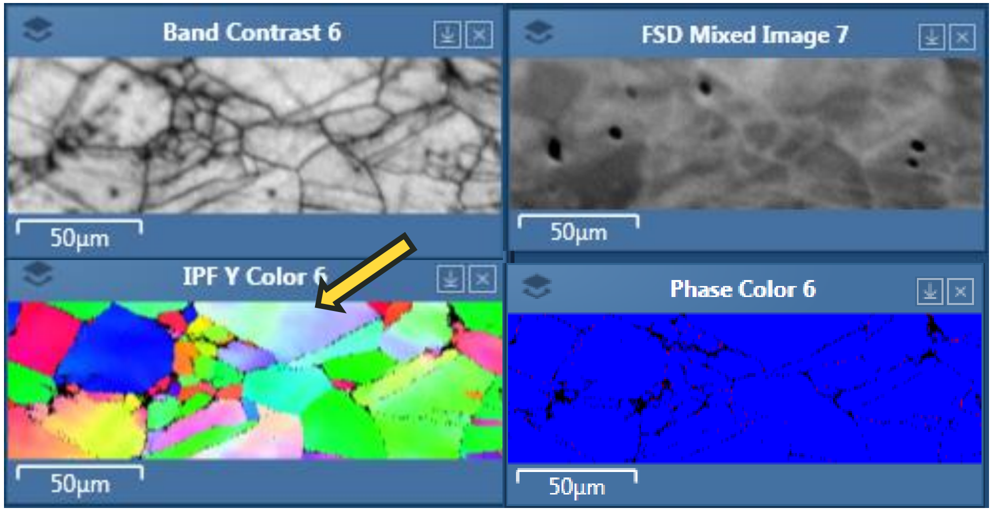

DENSITY AND CONDUCTIVITY

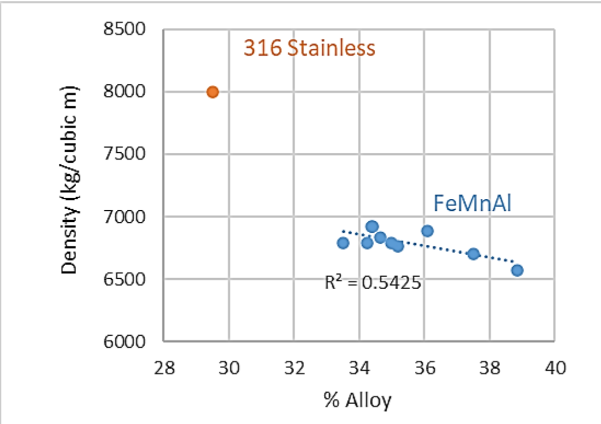

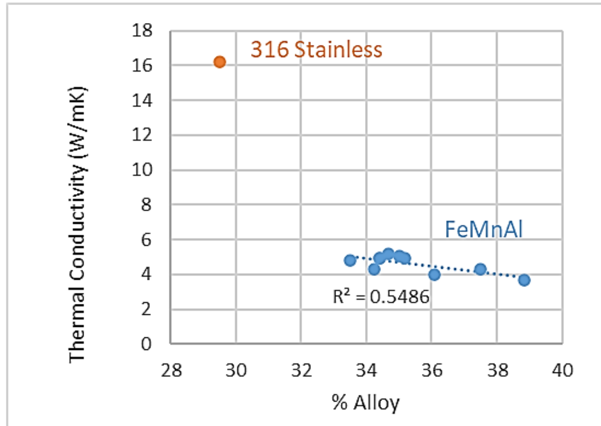

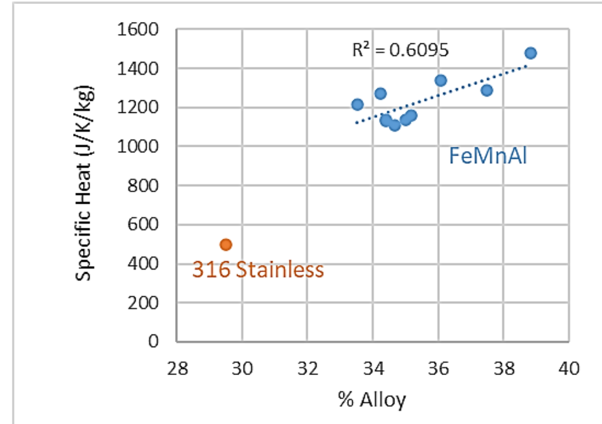

$$\epsilon_i = \frac{\rho c n}{-\left.\frac{\partial \sigma}{\partial T}\right|_{\epsilon,\dot{\epsilon}}}$$

ϵ_i = failure strain

ρ = density

c = specific heat capacity

n = strain hardening exponent

$\left.\frac{\partial \sigma}{\partial T}\right|_{\epsilon,\dot{\epsilon}}$ = change in stress as a function of temperature for constant strain and strain rate

$$\Gamma_{c0} = \frac{\rho c}{\alpha}\left(\frac{9\rho^3 c^2 \chi^3}{\sigma_y^3 \alpha^2 \dot{\epsilon}}\right)^{1/4}$$

Γ_{c0} = fracture energy

ρ = density

c = specific heat capacity

α = linear thermal softening

χ = thermal conductivity

σ_y = yield strength

$\dot{\epsilon}$ = strain rate

- **Density measure via ASTM D792 Specific Gravity method**
- **Thermal conductivity and effusivity were measured via ASTM D7984**
- **Specific heat was calculated from density, effusivity and conductivity**

EFFECT OF COMPOSITION

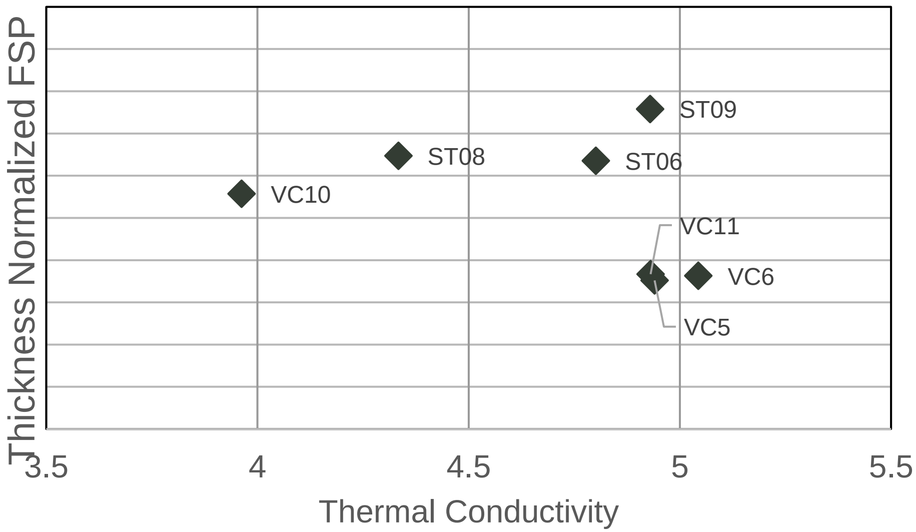

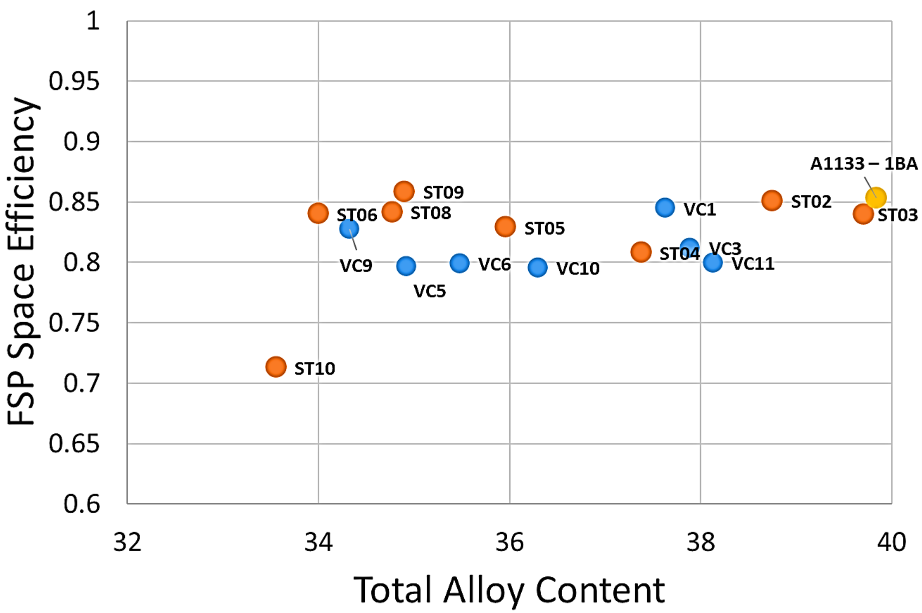

- **Fewer available data points for thermal conductivity due to limited plate**
  – Melting process may have a larger impact than limited variations in thermal conductivity
- **Trend becomes more ambiguous when looking at all points**
  – Total alloy content weakly correlates to thermal conductivity with R^2=0.54
  – With exception of ST10 plate, which fell well below target hardness, more homogeneous castings lead to better FSP performance
    - Industrially cast plate A1133 also higher performing

- **Evidence of recrystallization found, as well as deformation banding**
  - No “white banding” observed
  - Further EBSD work planned once ion mill reinstalled in new space
- **Failure via cleavage dominates large grains**
- **Branched cracking along ferrite bands**
- **Effects of plate homogeneity proved more impactful than compositional variations**
  - This will allow for processing kinetics to drive compositional selection versus performance requirements